Self-Coherent Camera: first results of a high contrast imaging bench in visible light

Marion Mas[a], Pierre Baudoz[a], Gérard Rousset[a], Raphaël Galicher[b], Jacques Baudrand[a].

[a] Laboratoire d'Etudes Spatiales et d'Instrumentation en Astrophysique (LESIA), CNRS, Observatoire de Paris, 5, place Jules Janssen, 92195 Meudon, France.

[b] Laboratoire Univers et Théorie (LUTH), CNRS, Observatoire de Paris, 5, place Jules Janssen, 92195 Meudon, France.

ABSTRACT

Extreme adaptive optics and coronagraphy are mandatory for direct imaging of exoplanets. Quasi-static aberrations limit the instrument performance producing speckle noise in the focal plane. We propose a Self-Coherent Camera (SCC) to both control a deformable mirror that actively compensates wavefront error, and calibrate the speckle noise. We create a reference beam to spatially modulate the coronagraphic speckle pattern with Fizeau fringes. In a first step, we are able to extract wavefront aberrations from the science image and correct for them using a deformable mirror. In a second step, we apply a post-processing algorithm to discriminate the companion image from the residual speckle field.

To validate the instrumental concept, we developed a high contrast imaging bench in visible light. We associated a SCC to a four quadrant phase mask coronagraph and a deformable mirror (DM) with a high number of actuators (32x32 Boston Michromachines MEMS). We will present this bench and show first experimental results of focal plane wavefront sensing and high contrast imaging. The measurements are compared to numerical simulations.

Keywords: instrumentation, high contrast imaging, high angular resolution, exoplanet, wavefront correction.

1. INTRODUCTION

Different techniques are used to characterize exoplanets. Radial velocity provides the minimum mass and orbital parameters of exoplanets studying the host star motions. Transits estimate the radius of a few planets orbiting very close to their star (a fraction of astronomical unit). For some of them, they also provide spectral informations, which helps characterizing their atmospheres. For further planets (more than a few AU) direct imaging is required. Nevertheless this technic is limited by two effects: the very high contrast (10^4 to 10^{10}) and the small angular separation (a fraction of arcsec) between the host star and its planet. A solution is to combine coronagraphy to an extreme adaptive optic system.

In the framework of the future European Extremely Large Telescope, new instrumental concepts are necessary to improve the sensitivity of the telescope down to rocky planets. Coronagraphs reduce stellar light but their performance is limited by aberrations, which induce speckles on the detector plane. The image of the companion is then lost in this speckle field. Differential imaging can be use to calibrate this speckle noise.[1] However, this is limited by static and differential aberrations of the optical system.[2] A more efficient solution is to first correct for the aberrations with a deformable mirror and then calibrate the residuals by such differential imaging. In that way, we propose to use a post coronagraphic method called the Self-Coherent Camera (SCC).[3] The principle has already been tested by numerical simulations.[4,5] At this time, we are working on an experimental high contrast imaging testbed to validate the SCC performance. In this paper, we first recall the principle and the formalism of the SCC in section 2. In section 3, we explain the calculation of the DM control matrix and we present results from numerical simulation. In section 4 we introduce the optical test bench. In section 5, we present preliminary results of wavefront estimation with the SCC coupled with deformable mirrors and a four quadrant phase mask coronagraph (FQPM).[6]

E-mail: marion.mas@obspm.fr, Phone number: +33 (0)1 45 07 75 12

Ground-based and Airborne Instrumentation for Astronomy III, edited by Ian S. McLean, Suzanne K. Ramsay, Hideki Takami, Proc. of SPIE Vol. 7735, 773566 · © 2010 SPIE · CCC code: 0277-786X/10/$18 · doi: 10.1117/12.857898

2. SCC PRINCIPLE

In this section we present the principle of the SCC. As explained in the introduction, aberrations induce speckles on the detector plane and then limit the coronagraph performance. The SCC concept is designed to overcome this speckle noise. A scheme of the principle is presented in Figure 1. Stellar light focuses on the coronagraphic mask in the first focal plane and is rejected outside of the geometrical pupil in the following pupil plane. A diaphragm (classical Lyot stop) stops this diffracted stellar light and defines the image channel. However a small part of the stellar energy goes through this channel because of phase and amplitude aberrations. As the companion is off axis, its image is not affected by the coronagraph, hence, all its energy passes through the image channel. To create the SCC reference pupil, we add a small hole in the Lyot stop plane. As the sole stellar light is diffracted by the focal coronagraphic mask, only stellar light goes through the reference channel. The two channels are recombined in a Fizeau scheme and spatial fringes are recorded on the detector. The reference light (stellar light) is only coherent with the residual stellar light of the image channel, but incoherent with the companion light. Thus, only the residual speckles are fringed and then encoded whereas the companion image is not. We call science image the image recorded by the detector. There are two ways to use the encoded image.

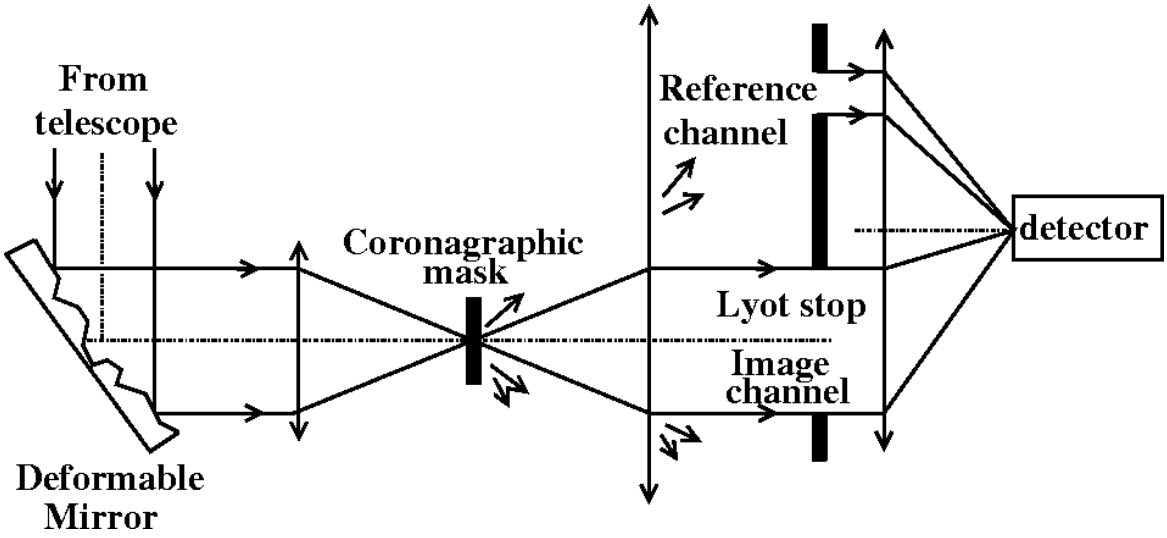

Figure 1. *Principle of the Self-Coherent Camera.*

In the first mode, the SCC is used as a wavefront sensor to estimate quasi-static aberrations in the pupil plane upstream from the coronagraph (phase and amplitude). This estimation is used to drive a deformable mirror placed upstream from the coronagraph. The image contrast is then enhanced. However, as the DM has a finite number of actuators the correction is not perfect, and some speckles still remain in the focal plane. A second mode of the SCC can be used to discriminate the companion image from these residuals in a post processing treatment.[4,5] In the following, we focus on the first mode and use the SCC as a focal plane wavefront sensor. We assume that there is no companion and study the contrast enhancing in the focal plane image. We also assume that their is no amplitude deformation in the pupil plane.

2.1 SCC image formation

In this section, we present the formalism to estimate the phase aberration ϕ with the SCC, as in a previous paper.[5] The complex amplitude of the electric field ψ'_S of the star upstream from the coronagraph in the pupil P can be written as

$$\psi'_S(\vec{\xi}) = P(\vec{\xi})\, exp(i\phi), \tag{1}$$

where $\vec{\xi}$ is the coordinate in the pupil plane. In the next focal plane, the complex amplitude of the residual phase A'_S is

$$A'_S(\vec{x}) = \mathcal{F}(\psi'_S)\, M(\vec{x}), \tag{2}$$

with $\mathcal{F}$ the Fourier transform operator, $\vec{x}$ the coordinate in the focal plane and M the mask function in the focal plane. In the Lyot stop plane, we add a small hole, a reference channel called R. We define by $L(\vec{\xi})$ the Lyot stop, $R(\vec{\xi})$ the reference stop and $\psi(\vec{\xi})$ the field amplitude transmitted by these two diaphragms

$$\psi(\vec{\xi}) = \mathcal{F}^{-1}\left(A'_S\right)\left(L(\vec{\xi}) + R(\xi - \vec{\xi}_0)\right). \tag{3}$$

We rewrite ψ as

$$\psi(\vec{\xi}) = \psi_S(\vec{\xi}) + \psi_R(\vec{\xi}) * \delta\left(\vec{\xi} - \vec{\xi_0}\right), \tag{4}$$

where $*$ is the convolution symbol, ψ_S and ψ_R are the complex amplitudes of the electric field of the residual stellar light and of the reference. From previous work [5, Eq. 2] the distance $\vec{\xi_0}$ between the two channels is

$$\| \vec{\xi_0} \| = \frac{D_L}{2}\left(3 + \frac{1}{\gamma}\right) 1.1 \tag{5}$$

D_L is the Lyot stop diameter and $\gamma = D_L/D_R$ with D_R the reference pupil diameter. We deduce the intensity I on the detector

$$I(\vec{x}) = \left|\mathcal{F}\left(\psi_S(\vec{\xi}) + \psi_R(\vec{\xi}) * \delta\left(\vec{\xi} - \vec{\xi_0}\right)\right)\right|^2 \tag{6}$$

Recalling that A_S is the Fourier transform of ψ_S and calling A_R the Fourier transform of the reference ψ_R, I can also be written as

$$I(\vec{x}) = |A_S(\vec{x})|^2 + |A_R(\vec{x})|^2 + 2\,Re\left(A_S(\vec{x})\,A_R^*(\vec{x})\,\exp\left(\frac{2i\pi\,\vec{x}.\vec{\xi_0}}{\lambda_0}\right)\right), \tag{7}$$

with λ_0 the wavelength. Speckles in A_S are spatially encoded with fringes on the detector plane.

2.2 Wavefront estimation

Assuming a small phase error ϕ, we can approximate Eq. 1 to

$$\psi'_S(\vec{\xi}) \simeq P(\vec{\xi})\,(1 + i\phi). \tag{8}$$

Under this assumption, we can write from Eq. 2

$$\mathcal{F}^{-1}\left(A'_S\right) = P\,\left(\mathcal{F}^{-1}(M) + i\phi * \mathcal{F}^{-1}(M)\right). \tag{9}$$

Using the rejection of the diffraction by the coronagraph, we have in the Lyot stop

$$\psi_S(\vec{\xi}) = i\left(\phi * \mathcal{F}^{-1}(M)\right)\,L(\vec{\xi}). \tag{10}$$

For a not undersized Lyot stop we deduce

$$\phi \simeq Im\left(\mathcal{F}^{-1}\left(\mathcal{F}\left(\psi_S\right)\,\left(\frac{1}{M}\right)\right)\right). \tag{11}$$

In the following, we develop the formalism to find an approximation of ψ_S (complexe amplitude of the electric field upstream from the coronagraph) in order to extract the estimated phase ϕ_{est} upstream from the coronagraph (Eq. 10).
Taking the Fourier transform of I (Eq. 7), we get three peaks in the correlation plane as shown in Figure 2. The two lateral peaks are conjugated. They contain information on the complex amplitude of the stellar speckles that are spatially modulated on the detector. To retrieve the phase errors, we select one of the lateral peaks, center it and apply a Fourier transform. We assume a narrow spectral bandwidth and neglect the chromatism effect in Eq. 7.[5] We obtain the complex

$$I_-(\vec{x}) = A_S(\vec{x})\,A_R^*(\vec{x}) \tag{12}$$

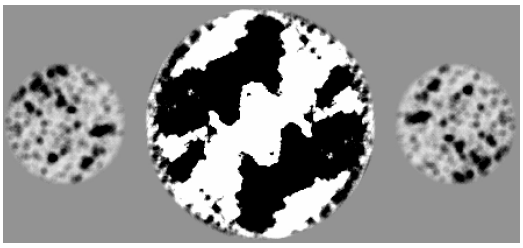

Figure 2. *Correlation peaks of the spatially modulated focal plane image recorded by the detector. It corresponds to the Fourier transform of the SCC interferential image. Left peak:* $\mathcal{F}^{-1}\left(A_S\, A_R^*\right)$*, right peak:* $\mathcal{F}^{-1}\left(A_S^*\, A_R\right)$*, central peak:* $\mathcal{F}^{-1}\left(|A_S|^2 + |A_R|^2\right)$

The estimated pupil complex amplitude $\psi_{S_{est}}$ downtream from the coronagraph is

$$\psi_{S_{est}}(\vec{\xi}) = \mathcal{F}^{-1}\left(\frac{I_-}{A_R^*}\right). \tag{13}$$

From Eqs. 11 and 13, for a not undersized Lyot stop, we approximate the phase ϕ_{est} upstream from the coronagraph

$$\phi_{est} \simeq Im\left(\mathcal{F}^{-1}\left(\frac{I_-}{A_R^*}.\frac{1}{M}\right)\right). \tag{14}$$

The impact of the Lyot stop size on the phase estimation is discussed in section 3.2.

3. NUMERICAL SIMULATIONS

In this section, we present results from numerical simulation of the SCC coupled with a four quadrant phase mask coronagraph and a deformable mirror (DM). This simulation tool is developed in parallel of our bench implementation. We study the SCC wavefront sensor estimation and the correction by a DM. We assume a finite number of actuators on the DM.

3.1 Computation of the DM control matrix

To define the best parameters to apply on the bench, we developed a numerical tool to simulate the different steps we intend to follow on the test bench. For example, since we plan to apply phase correction using a control matrix calculated from a recorded interaction matrix, we need to simulate both matrices for the finite number of actuators we have on our DM. We call them M_{int} and $M_{control}$.
We will consider here that the DM is able to produce Zernike polynomials[7] as its actuator surface deformations. We define the DM as the set of the $N_{zn} - 1$ wavefront deformations ϕ_i given by

$$\phi_i = a_i Z_i, \;\; i = 2, ...N_{zn}, \tag{15}$$

where Z_i is the i^{th} Zernike polynomial and a_i a coefficient in radian.
To calibrate the interaction matrix in the simulation, we apply such ϕ_i in the pupil and compute the formed SCC image. We assume a small phase in order to make the assumption in Eq. 8. Hence, we take $a_i = 10^{-3}$ radian.
Now we consider that the estimation of the phase ϕ_{est} (Eq. 14) from the recorded SCC image is expanded on the Zernike polynomial basis to build the measurement vector. Therefore we call M_{int_i} the matrix composed by the $N_{zn} - 1$ first Zernike coefficient vectors obtained from each estimated phase $\phi_{i_{est}}$. We have

$$M_{int_{i,j}} = \frac{\int\int \phi_{i_{est}}.Z_j\, d\vec{\xi}}{\int\int P\, d\vec{\xi}}, \;\; i = 2, ...N_{zn}, \;\; j = 2, ...N_{zn}. \tag{16}$$

We then deduce the control matrix

$$M_{control} = \left(M_{inter}^T \,.\, M_{inter}\right)^\dagger \,.\, M_{inter}^T. \tag{17}$$

We correct for a known initial wavefront aberration ϕ^C using $M_{control}$. We define ϕ^C as a single Zernike multiplied by a coefficient C (in radian). We choose C to have a small wavefront error. To simulate a situation close to the real conditions on the bench, we add a white noise on the SCC image in Eq. 7, on the detector plane. We set the noise level in function of the SCC image maximum. We estimate the phase ϕ_{est}^C (Eq. 14) in the pupil plane upstream from the coronagraph. We then expand this estimated phase on the Zernike polynomial base composed by the $N_{zn} - 1$ Zernike polynomials and we note this vector $Proj = (Proj_j)$ with

$$Proj_j = \frac{\int\int \phi_{est}^C . Z_j \, d\vec{\xi}}{\int\int P \, d\vec{\xi}}, \;\; j = 2, ...N_{zn}. \tag{18}$$

We then compute the coefficients (α_j) of the correction vector

$$(\alpha_j) = M_{control} \,.\, Proj \tag{19}$$

and the variance σ^2 of residual errors using the zernike coefficients

$$\sigma = \sqrt{\sum_{i=2}^{N_{zn}} (a_i - \alpha_i)^2}. \tag{20}$$

3.2 Performance

In this section, we present preliminary results using our simulation. We can change different parameters to study the impact of the Lyot stop size, the parameter γ (defined in Eq. 5) and the white noise (added in the SCC focal plane image) on the SCC performance.
We consider a SCC device operating in visible light ($\lambda = 630$ nm). We test the impact of the Lyot stop size, the parameter γ (defined in Eq. 5) and the white noise (added in the SCC focal plane image) on the SCC performance. We plot the normalized residual errors (σ/C) in Figure 3. We recall that D_L is the Lyot stop diameter (in percentage of the diameter pupil size), and N the white noise (in percentage of the SCC image maximum). In the simulation, we test the SCC performance with

- $D_L = 1$, 0.90, 0.85,
- $\gamma = 50$, 20,
- $N = 0$, 0.005, 0.01, 0.02, 0.03, 0.1, 0.5, 1, 5.

The curves represent the evolution of the relative residual phase errors (after one correction) with respect to the white noise. With this simulation, we can predict the optimal combination of the parameters to configure the bench in order to optimize the SCC performance. For example, the size D_R of the reference pupil R impacts the pupil aberration estimation. If the reference pupil diameter gets larger ($\gamma \lesssim 20$), the number of unestimated spatial frequencies of the pupil aberrations increases and the SCC performance gets worse. In the presented simulations, there are the zero values of A_R inside the field of the image. In the computation of ϕ_{est}, this leads to noise amplification in Eq. 14. We will have in a near future to get rid of such noise amplification by using optimum estimation approach. The Lyot stop size diameter D_L has also an impact on the phase estimation. As we estimate the complex amplitude $\psi_{S_{est}}$ (Eq. 13) in the Lyot stop pupil to define the wavefront ϕ_{est}, the smaller the Lyot stop diameter is, the worse the estimation is, hence, the worse the correction of the wavefront is too. Preliminary results presented here call for an optimization of the intrumental parameters and a more evolved data processing algorithm to better estimate the aberration ϕ.

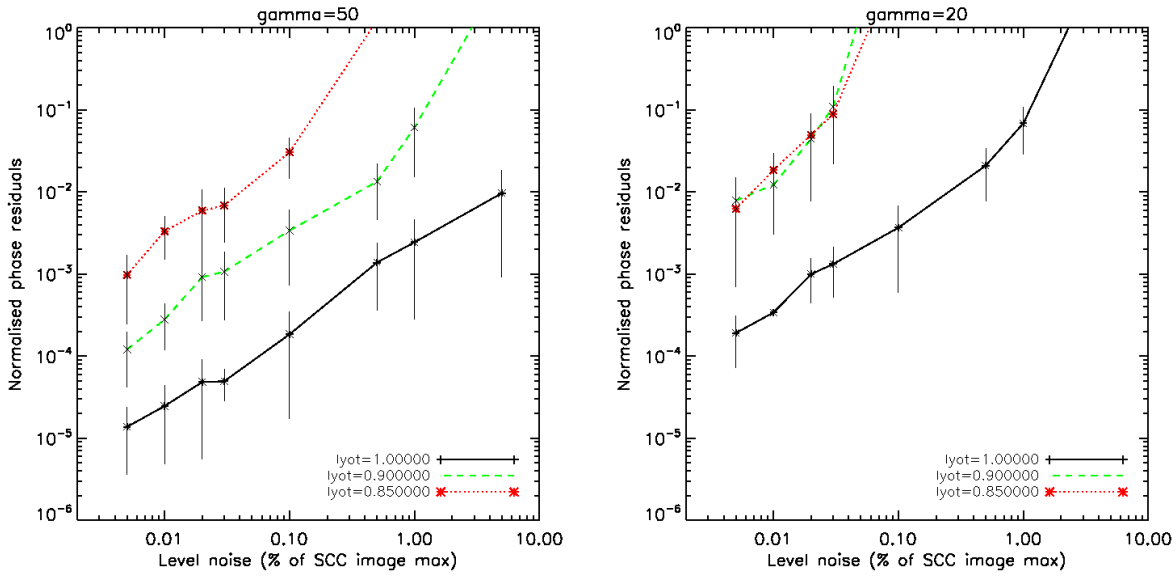

Figure 3. *Evolution of the normalised phase residual with respect to the level of noise. Left:* $\gamma = 50$*, right:* $\gamma = 20$.

4. EXPERIMENTAL TEST BENCH

In this section we introduce the high contrast imaging bench we developed at LESIA to test the performance of the SCC in laboratory condition. We work with a monochromatic laser light. The bench includes off axis parabolas, a tip tilt mirror and a deformable mirror, a four quadrant phase mask coronagraph and an imaging CCD detector. In order to minimize dynamical aberrations in the lab, we add athermal enclosure around the bench. This bench is shown in Figure 4.

4.1 The laser

We work in visible light. The laser is centered on $\lambda_0 = 635$ nm with a relative spectral bandwidth lower than 1% and a power of 2.5 mW.

4.2 Adaptive mirrors

4.2.1 The tip tilt mirror

The tip tilt mirror is made of two axis gimbal mounts equiped with piezoelectric actuators. The maximum stroke is 2 mrad and the positionning accuracy is 0.16 μrad.

4.2.2 Deformable mirror

We first used OKO DM with 37 actuators. We did first calibration of the bench and developed the driving software of the bench with this DM.[8] We have recently implemented a 32x32 actuators Boston Micromachine MEMS deformable mirror. These two DMs are electrostatic, their actuators response is quadratic with the voltage. Deformable and tip tilt mirrors are driven by a labview interface. Main characteristics of these two DM are summarized in Table 1.

4.3 The CCD detector

We use a detector ATV Pike F -032B with 680 by 460 pixels which works in visible light. The pixel size is 7.4 μm. The sampling og the image is $\lambda/6.8D$.

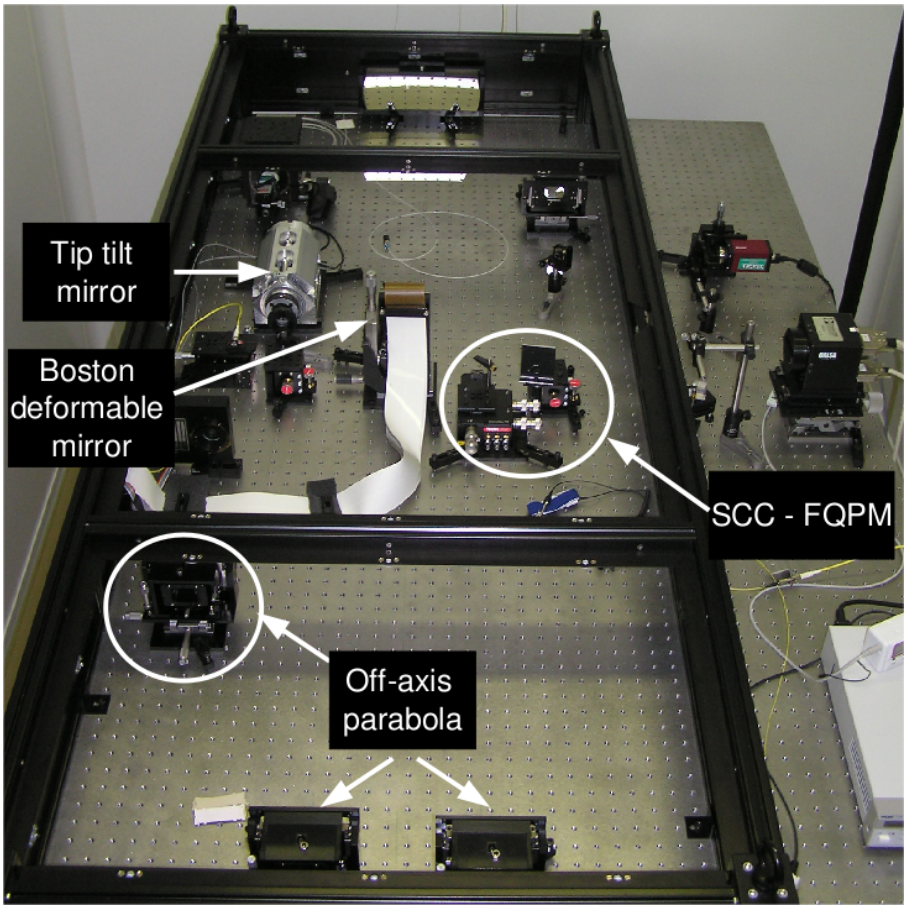

Figure 4. *High contrast imaging bench with top pannels of the bench enclaves removed*

SCC	OKO DM	Boston Micromachines DM
Number of actuators	37	32x32
Inter actuator space	1.8 mm	300 μm
Pupil diameter	10 mm	9 mm
Maximum stroke	540 nm	1500 nm
Inter actuator coupling	60%	25% and $< 30\%$
Bandwidht (DM + electronic)	0.5 Hz	> 2 kHz
Maximum voltage	266 V	295 V

Table 1. *Main characteristics of DMs.*

5. PRELIMINARY EXPERIMENTAL RESULTS

5.1 With the OKO DM

The first goal of the experimentation was to measure the wavefront upstream from the coronagraph with the SCC. To be sure that the wavefront is well estimated by the SCC, we added a second optical path using a beam splitter before the coronagraph and we used a Shack-Hartmann wavefront sensor to measure the phase aberration simultaneously with the SCC. Pulling each actuator of the DM one by one, we induce, for each actuator pulled, a deformation of about 90 nm of the mirror membrane. We make differential measurement (this wavefront is measured with both the SCC and the Shack-Hartmann simultaneously). Figure 5 represents the image on the

CCD of the estimated wavefront. The shape of the wavefront estimated with the SCC is very similar to the

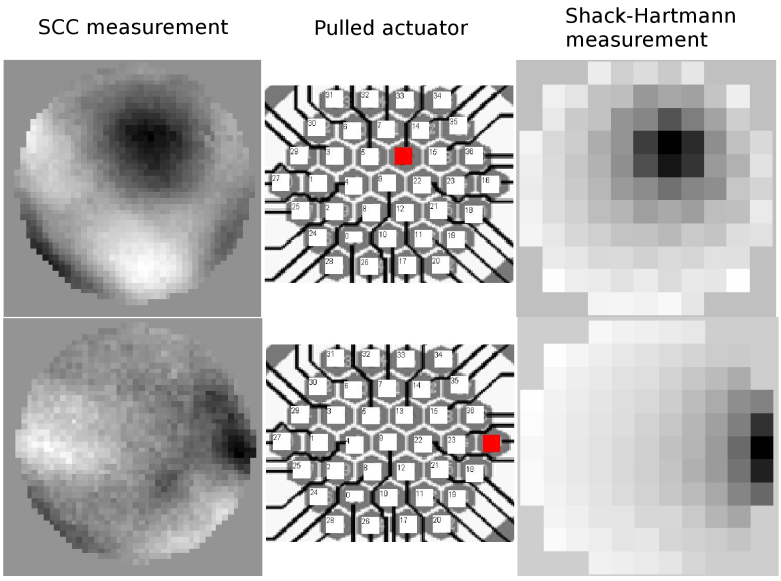

Figure 5. *Left: wavefront measurement with the SCC, middle: pulled actuator, right: wavefront measurement with a Shack-Hartmann*

wavefront measured with the Shack-Hartmann. We used this DM to do the alignements, to calibrate the bench and to develop the software which control the full experiment.

5.2 With the 32x32 Boston Micromachines DM

In this section, we show results from both experiment and numerical simulation of the bench using the SCC coupled with the 32x32 Boston Micromachines DM and the four quadrant phase mask coronagraph. As described in section 2.2, we want to study a wavefront measurement with the SCC. First step of the experiment is to control the DM with labview interface and compare the shape of the wavefront deformation with simulation of the bench.

5.2.1 Experiment

On the bench, we pull all the actuators at 70% of their maximum stroke to control the DM in pull-push mode. Then, we pull each actuator one by one to 65% and 75% of its maximum stroke applying alternatively two voltages. For each actuator, we have two wavefront deformations estimated with the SCC. As the DM is not flat, in order to measure influence functions of the deformable mirror, we make differential measurement between the two voltages. We call D, D_L and D_R the diameter of the entrance pupil, the Lyot stop and the reference and we recall that $\gamma = D_L/D_R$. On the bench we have:

- $D = 9$ mm,
- $D_L = 6.5$ mm,
- $D_R = 1.5$ mm,
- $\gamma = 4.3$

From the interferential image we estimate $Im\left(\mathcal{F}^{-1}\left(I_-/M\right)\right)$, which is the convolution of the phase error ϕ_{est} (that we are looking for) with the reference pupil.

5.2.2 Simulation of the bench

In the simulation, we approximate the influence functions of the deformable mirror with a gaussian function.[9] Multiplying the influence functions by a positive or negative coefficient, we simulate a deformation of the membrane with the voltage. We compare results from both the simulation and the experiment in Figure 6. We

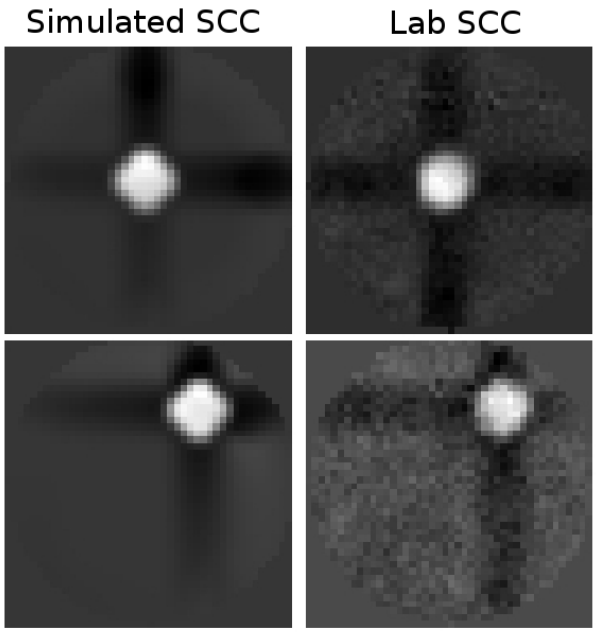

Figure 6. *Left:wavefront measurement with simulated SCC, wavefront measurement with Lab SCC*

find the same structure (due to the four quadrant phase mask coronagraph) with both the simulation and the experiment. As we know what we estimate with the SCC in simulation, we can understand better what happens on the bench and be able, in a near future time, to optimize the control of the DM to get high contrast images.

6. CONCLUSION

In this paper, we have recalled the principle of the SCC and developed the formalism used to simulate real experimental data. We have introduced the high contrast imaging bench. We described the simulation tool which will enable us to better understand and predict the data from the bench. First experimental results on the phase estimation done with a OKO 37 actuators deformable mirror have been presented. Then a comparison was done between laboratory results and real simulation of the bench on phase estimation with a 32x32 deformable mirror. Next step will be to drive the deformable mirror in order to correct this wavefront error with the DM. For this, we need to flatten perfecly the DM knowing exactly influence function. This work is under study.

REFERENCES

[1] Racine, R., Walker, G. A. H., Nadeau, D., Doyon, R., and Marois, C., "Speckle Noise and the Detection of Faint Companions," *The Publications of the Astronomical Society of the Pacific* **111**, 587–594 (May 1999).

[2] Cavarroc, C., Boccaletti, A., Baudoz, P., Fusco, T., and Rouan, D., "Fundamental limitations on Earth-like planet detection with extremely large telescopes," *Astronomy and Astrophysics* **447**, 397–403 (Feb. 2006).

[3] Baudoz, P., Boccaletti, A., Baudrand, J., and Rouan, D., "The Self-Coherent Camera: a new tool for planet detection," in [*IAU Colloq. 200: Direct Imaging of Exoplanets: Science & Techniques*], C. Aime & F. Vakili, ed., 553–558 (2006).

[4] Galicher, R. and Baudoz, P., "Expected performance of a self-coherent camera," *Comptes Rendus Physique* **8**, 333–339 (Apr. 2007).

[5] Galicher, R., Baudoz, P., Rousset, G., Totems, J., and Mas, M., "Self-coherent camera as a focal plane wavefront sensor: simulations," *Astronomy and Astrophysics* **509**, A31+ (Jan. 2010).

[6] Rouan, D., Riaud, P., Boccaletti, A., Clénet, Y., and Labeyrie, A., "The Four-Quadrant Phase-Mask Coronagraph. I. Principle," *The Publications of the Astronomical Society of the Pacific* **112**, 1479–1486 (Nov. 2000).

[7] Noll, R. J., "Zernike polynomials and atmospheric turbulence," *Journal of the Optical Society of America (1917-1983)* **66**, 207–211 (Mar. 1976).

[8] Mas, M., Baudoz, P., Galicher, R., Rousset, G., Baudrand, J., Coton, C., and Assémat, F., "Status of the LESIA High Contrast Bench development in the framework of the E-ELT," in [*Adaptative Optics for Extremely Large Telescopes*], (2010).

[9] Huang, L., Rao, C., and Jiang, W., "Modified gaussian influence function of deformable mirror actuators," *Optical Society of America Journal* **16**, 108 – 114 (2008).